




Tunneling electronic excitations spatial mapping of a single graphene nanoribbon on Ag(111)

Umamahesh Thupakula ^{1,*} We-Hyo Soe ^{1,†} Xavier Bouju ¹ Erik Dujardin,^{1,2} and Christian Joachim^{1,3}

¹*Centre d'Élaboration de Matériaux et d'Études Structurales (CEMES), Centre National de la Recherche Scientifique (CNRS), Université de Toulouse, 29 Rue J. Marvig, BP 94347, 31055 Toulouse Cedex, France*

²*Laboratoire Interdisciplinaire Carnot de Bourgogne, CNRS UMR 6303, Université de Bourgogne Franche-Comté, 9 Avenue A. Savary, 21078 Dijon, France*

³*International Center for Materials Nanoarchitectonics (WPI-MANA), National Institute for Materials Science (NIMS), 1-1 Namiki, Tsukuba, Ibaraki 305-0044, Japan*



(Received 10 March 2023; revised 24 June 2023; accepted 1 August 2023; published 31 August 2023)

Using low temperature scanning tunneling microscopy (STM), spectroscopy (STS), and precise dI/dV mapping in combination with density-functional theory-parametrized semiempirical calculations, we report and discuss the origin of tunneling electronic excitations that occur along a seven-carbon-atom-wide armchair graphene nanoribbon (7-aGNR) physisorbed on Ag(111) as compared to a reference on Au(111) surface. On both surfaces, on-surface synthesized 7-aGNRs of variable lengths are selectively chosen for performing the STM and STS (dI/dV) excitation mapping along a truly isolated molecule. For exactly the same 7-aGNR molecule length, the difference in work functions between Ag(111) and Au(111) generates different edge states electronic configuration that result in a curved molecular conformation on Ag(111) and a strictly flat one on Au(111). At the interface between the 7-aGNR and Ag(111), this curved conformation produces an additional set of quantum-box-like tunneling resonances that partially mix with the intrinsic 7-aGNR tunneling excitations.

DOI: [10.1103/PhysRevMaterials.7.085005](https://doi.org/10.1103/PhysRevMaterials.7.085005)

I. INTRODUCTION

The molecular conformation and tunneling electronic excitation spectrum of an on-surface synthesized graphene nanoribbon (GNR) [1–3] are vulnerable to surface-induced perturbations such as substrate polarization [4], charge transfer [5], and/or molecular structural deformations [6]. A free standing GNR predominately interacts with an atomically flat metallic surface through weak van der Waals (vdW) forces [7,8]. The alignment of the GNR electronic structure with respect to the Fermi level (E_F) of the metallic surface can generate charge screening and renormalization effects [4,5,9]. These interactions introduce new electronic excitations, which are sometimes intimately entangled with the intrinsic molecular electronic structure in locally probed signals [10]. In order to capture the intrinsic electronic properties of GNRs lying on a metallic surface or to avoid the entanglement effects resulting from such interactions with the metal, different configurations have been tested in the past: STM molecular manipulating the GNR onto an insulating NaCl atomic layer spacer [11], intercalating one atomic layer of a foreign element [12], and direct on-surface synthesis of the GNR on an insulating substrate [13,14]. However, the charging effects occurring, for example, in a GNR/NaCl/Au(111) junction configuration or the positioning of the GNR molecular electronic states relative to the insulating substrate make these composite systems [15] more complex to interpret and model,

which usually fails to provide a precise characterization and understanding of the tunneling electronic excitation spectrum of an adsorbed GNR on a surface.

Here, we compare highly resolved tunneling electronic excitation spectra of a seven-carbon-atom wide armchair GNR (7-aGNR) obtained by scanning tunneling microscopy (STM) on a Ag(111) and on a standard Au(111) surface. Exploring a few eV around E_F , we spatially map the tunneling dI/dV resonances of a 7-aGNR on Ag(111) and on Au(111) with respect to the vacuum level. We reveal that the two different surfaces generate different electronic configurations of the edge states (ESs) of the same length 7-aGNR, owing to the difference in their work function. A striking feature is the curved conformation adopted by the 7-aGNR on Ag(111) whereas it remains strictly flat on Au(111). As a consequence of this conformational difference, peculiar electronic effects at the interface between a 7-aGNR and the Ag(111) surface are uncovered and discussed. We also find that the Ag(111) Shockley surface electrons are confined and quantized laterally under the curved 7-aGNR. By comparing the dI/dV spectra and maps on the two metallic surfaces, we are able to separate the tunneling electronic excitations specific to the 7-aGNR/Ag(111) interface from the ones intrinsically borne by the 7-aGNR molecule.

II. MATERIALS AND METHODS

A. Materials

All samples were prepared in the preparation chamber of a low-temperature ultrahigh vacuum (LT-UHV) 4-STM instrument [16]. Ag(111) and Au(111) single crystal surfaces (Mateck GmbH) were first cleaned under UHV conditions

*Corresponding author: umamahesh.thupakula@cemes.fr

†Present address: Center for Quantum Nanoscience, Institute for Basic Science (IBS), Ewha Womans University, Seoul 03760, Korea; soe.we-hyo@qns.science

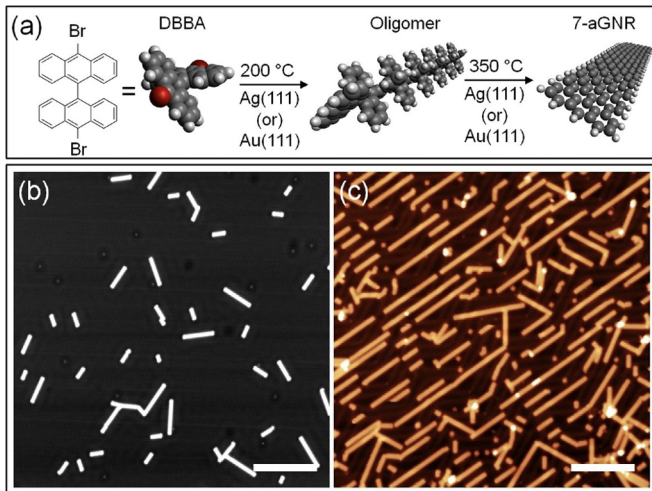


FIG. 1. On-surface synthesis of 7-aGNRs on Ag(111) and Au(111) surfaces. (a) Schematic molecular model illustration of the two-step on-surface synthesis approach of 7-aGNRs using DBBA monomers. Large scale STM images of on-surface synthesized 7-aGNRs, (b) on Ag(111), and (c) on Au(111). Scale bars are 20 nm. Scan parameters are -2 V/100 pA.

by repeated cycles of Ar^+ ion sputtering at 1.0 keV and $\sim 10^{-6}$ mbar for about 10 min and subsequent annealing at about 740 K for 1 h. These single crystal surfaces were checked for cleanliness by using one of the scanning tunneling microscopes of our LT-UHV 4-STM operated at sample temperatures of ~ 4.5 K. Monomer precursors “10,10'-dibromo-9,9'-bianthryl (DBBA, >98%)” from Aldrich were thermally evaporated at 160°C onto the clean surfaces of Ag(111) and Au(111) from the quartz crucible of a Kentax thermal evaporator (Knudsen cell), while the substrates were kept below 40°C and approximately 50 mm away from the evaporation source. These precursor molecules were out gassed for more than 24 h in the UHV preparation chamber of our LT-UHV 4-STM to remove the residual contaminants prior to their depositions onto Ag(111) and Au(111) surfaces.

B. On-surface synthesis of 7-aGNRs

On-surface synthesis of 7-aGNRs was carried out on Ag(111) and, for comparison, on Au(111) by following the standard two-steps on-surface synthesis approach for DBBA monomer precursor molecules, by annealing the samples 10 min each at 200 and 350°C in UHV conditions [17]. This standard approach for DBBA monomers follows the Ullmann coupling reaction between the monomers at the cleaved bromine sites resulting in polyanthryl oligomers at the first annealing step (200°C) and then the cyclodehydrogenation of the polyanthryl oligomers at the second annealing step (350°C), producing the 7-aGNRs [Fig. 1(a)]. This on-surface chemical reaction procedure results in a broad length distribution of well isolated 7-aGNRs from as small as a one-monomer unit equivalent to as long as several tens of monomer units long on both metallic surfaces. This allows us to selectively choose the well-defined 7-aGNR length (in the units of number of monomer precursor molecules) for further

characterization of 7-aGNR length dependent tunneling electronic excitation characteristics (dI/dV spectra and maps).

C. Characterization of 7-aGNRs

STM imaging and scanning tunneling spectroscopic (STS) characteristics (also referred to as dI/dV spectra and maps) of 7-aGNRs were precisely characterized *in situ* with a *Scientia Omicron* 4-STM instrument. STM and STS were recorded with electrochemically etched PtIr (Ir: 20%) tips and in constant-current configuration using a lock-in detection technique (frequency ~ 460 Hz, modulation voltage = 20 mV). Prior to the STS characterization of well isolated individual and selected 7-aGNR, the STM tip apex was checked for its purity and cleaned whenever necessary by probing the Au(111) or Ag(111) surface state characteristics. A pure STM tip apex is always characterized by the steplike dI/dV characteristic at energetic positions of ~ -50 mV for Ag(111) surface and ~ -460 mV for Au(111) surface.

D. Theoretical calculation details

To compute the conformational differences of a 7-aGNR on Ag(111) and Au(111) surfaces, semiempirical calculations were performed using the ASED+ code, including van der Waals interactions and a non-standard three-body term. A semiempirical approach with the extended Hückel molecular orbital theory constitutes the core of the ASED-MO method [18,19]. The ASED+ code [20] is a powerful numerical tool that describes reasonably well the structural properties of various types of molecules adsorbed on surfaces or in the gas phase [21–24]. For all the calculations, the surface atoms are kept frozen and no surface reconstruction is taken into account. Standard density-functional theory (DFT) codes are not appropriate in the present case due to expensive computational needs to address the 7-aGNR adsorption. However, ASED+ was parametrized using DFT calculations for small unit cell surfaces. This parametrization is described in Ref. [20] where a non-standard three-body term was introduced and the standard Wolfsberg-Helmholtz semiempirical parameters optimized accordingly.

III. RESULTS AND DISCUSSION

A. Electronic tunneling excitation spectra and maps of a 7-aGNR on Ag(111) and Au(111)

Figures 1(b) and 1(c) presents large scale STM images of on-surface synthesized 7-aGNRs on Ag(111) and, for comparison, on Au(111) using a two-step annealing approach. The STM images present different 7-aGNR coverages on Au(111) and Ag(111) starting from different initial monomer concentrations [0.1 monolayer on Ag(111) and 1.5 monolayer on Au(111)] at room temperature surface deposition conditions. A well isolated 7-aGNR of predefined length (in the number of DBBA monomer molecule units) can be selectively chosen for the precise measurement of tunneling electronic excitations occurring within an individual 7-aGNR molecule. Many electronic tunneling resonances are captured at both positive and negative bias voltages on an Ag(111) surface as the STM tip apex is positioned along the armchair side of a 7-aGNR comprising five-monomer units (i.e., ten anthracene

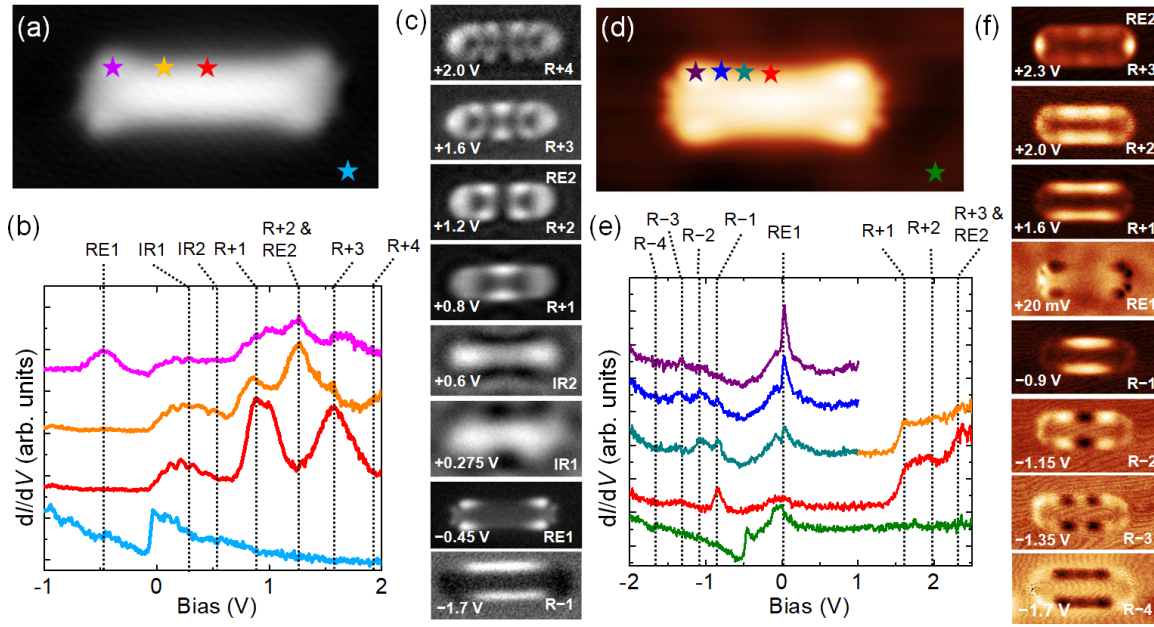


FIG. 2. Electronic tunneling excitation resonances of a five-monomer-units-long 7-aGNR on Ag(111) and Au(111). (a) STM image of a five-monomer-units-long 7-aGNR on Ag(111) surface ($V_{\text{bias}} = +20$ mV, $I = 20$ pA). (b) Corresponding dI/dV spectra recorded at different positions [marked with colored stars in (a)] along the armchair side. Several electronic resonances of the 7-aGNR are resolved and highlighted with vertical dotted lines. (c) Corresponding dI/dV maps recorded at the tunneling resonance voltages revealed in (b). They showcase the electronic behavior of 7-aGNR on the Ag(111) surface. RE1 and RE2 represent the low-bias and high-bias ESs of the 7-aGNR, respectively. IR1 and IR2 represent the interface resonances. (d)–(f) STM image and dI/dV characteristics revealing the electronic behavior of the same length (five-monomer-units-long) 7-aGNR on the Au(111) surface similar to that on the Ag(111) surface presented in (a)–(c), respectively. Scan sizes are $8 \text{ nm} \times 4 \text{ nm}$ (length \times height). Ag(111) and Au(111) reference dI/dV spectra are presented in blue and green curves in (b) and (e), respectively.

long) as shown in Figs. 2(a)–2(c). At positive (respectively negative) bias with respect to E_F , these resonances, labeled as $R + n$ (respectively $R - n$) with an integer $n \geq 1$, are the elastic electronic tunneling excitations when the STM current tunnels through the 7-aGNR (see Supplemental Material [25] Sec. 1 for more details about negative bias $R - n$ resonances). Each resonance results from the contribution of the electron (respectively hole) transfer through mono-electronic channels of the 7-aGNR at positive (respectively negative) bias voltage with respect to the grounded Ag(111) surface. In the dI/dV spectra, RE1 resonance corresponds to the well-known edge state (ES) resonance intrinsic to a 7-aGNR [2]. On either side of the E_F , the dI/dV maps recorded at the first delocalized resonances ($R - 1$ and $R + 1$) and at the end-localized resonance (RE1) of the 7-aGNR can be described in first approximation by their corresponding highest occupied molecular orbital (HOMO), lowest unoccupied molecular orbital (LUMO), and spin occupied molecular orbital (SOMO) mono-electronic probability distribution in space [21]. The resonances noted as IR_n ($n \geq 1$, integer) at +0.275 and +0.6 V originate from the surface quantum-box-like effect generated only at the 7-aGNR/Ag(111) interface due to the curved molecular conformation, as discussed in Sec. III D. Higher bias voltage maps ($R + n$ and $R - n$ with $n \geq 2$) must be described by a superposition of several virtual hole and electron transfer processes through the 7-aGNR. In principle, each resonance involves many molecular orbitals below the HOMO and above the LUMO levels and belongs to the active quantum state space describing the electronic tunneling effect through

the 7-aGNR in a complete configuration interaction (CI) approach [26]. As a consequence, the best dI/dV map contrast for each resonance (as assessed by the contrast between the minima and maxima of a given differential conductance map) is not obtained at the corresponding peak position of a dI/dV resonance but at a slightly shifted bias [27]. Indeed, following the principle above, all the dI/dV mappings reported in this investigation are recorded at up to ~ 50 -mV-shifted bias voltages compared to the spectral peak positions.

Figures 2(d)–2(f) present the STM image and STS characteristics recorded on an Au(111) surface for a 7-aGNR with the exact same length of five-monomer units (ten anthracene long). Similarly to other dI/dV characteristics of 7-aGNR on Au(111) reported in the literature [armchair eigenmodes ($R + n$ and $R - n$) and low-bias ESs (RE1)] [28], several additional resonances ($R \pm n$ and RE2) are clearly observed and spatially resolved/mapped. These measurements were performed far above and below E_F to gather a complete STS reference in the experimentally allowed bias voltage window before destabilization of the STM tip apex. Here again, it should be noted that the measured tunneling current intensity of a selected dI/dV resonance and map pixel results from the quantum superposition of all contributions involved in an elementary hole (electron) transfer event through the 7-aGNR electronic cloud. The corresponding dI/dV maps recorded at these resonances bear the combined characteristics of the main spatial contribution of the mono-electronic eigenmodes involved in the respective virtual (electron or hole) tunneling excitations quantum superposition of the CI [26]. Nonetheless, similarly

to the Ag(111) case, these eigenmodes on Au(111) can be considered as a virtual hole (respectively electron) occupation in a HOMO $- n$ (respectively LUMO $+ n$) molecular orbital. In particular, the bias difference between $R - 1 = -0.9$ eV and $R + 1 = +1.6$ eV gives a quasi-single-particle electronic gap of ~ 2.5 eV (i.e., the HOMO-LUMO gap), consistent with previously reported values for 7-aGNRs on-surface synthesized on Au(111) [1,5].

Notably, on Au(111), the electronic eigenmodeslike behavior observed from the dI/dV maps (for $R - n$ and $R + n$) in Fig. 2(f) reveal that the highest dI/dV intensities are mainly located at the armchair side with null amplitude in the interior part of the 7-aGNR. This particular spatial behavior of 7-aGNR dI/dV maps is well documented by Söde *et al.* [29], where the authors illustrated how a specific STM tip height trajectory in a constant-current or a constant-height mode STS measurement affects the respective dI/dV intensity maxima concentrating at the armchair sides or inside of the 7-aGNR, respectively. This is in good agreement with our armchair side localization of $R \pm n$ electronic eigenmodes captured in constant-current configuration. Unlike on the Au(111) surface, our data on the Ag(111) show non-negligible dI/dV intensities inside of the 7-aGNR with intriguing dI/dV spatial map patterns, which follow a different electronic eigenmodeslike character as can be seen in Fig. 2(c). Below, we focus on revealing, step by step, the origin of this distinct tunneling electronic excitation behavior within the 7-aGNR on the Ag(111) surface as compared to that on the Au(111) surface.

In contrast to Au(111), only one electronic resonance is captured from the 7-aGNR on Ag(111) at negative bias voltage ($R - 1$ at -1.7 V), i.e., below RE1 (see Supplemental Material [25] Sec. 1 for more details). The corresponding dI/dV map [at -1.7 V in Fig. 2(c)] exhibits a uniform bright contrast at the armchair sides resembling the $R - 1$ dI/dV map [at -0.9 V in Fig. 2(f)] of the same length 7-aGNR on Au(111). Remarkably, on Ag(111), the difference between $R - 1$ and $R + 1$ is found to be ~ 2.5 eV, which matches exactly the quasi-single-particle gap of 7-aGNR observed on Au(111). However, STS measurements carried out on Ag(111) for 7-aGNR with different lengths reveal that the position of the $R - 1$ resonance remains fixed at -1.7 V and is independent of the 7-aGNR length (see Supplemental Material [25] Sec. 1 for more details). It results from the opening of a hole transfer channel coming from a topological length invariant mono-electronic state contribution to the 7-aGNR ground electronic state on Ag(111) located well below E_F [30]. On Au(111), this low lying virtual excitation channel is not accessible in our present LT-UHV 4-STM setup. Compared to the 7-aGNR dI/dV spectra/maps on Au(111) presented in Figs. 2(e) and 2(f), more dI/dV resonances/maps were recorded on Ag(111) at positive bias voltage in Figs. 2(b) and 2(c). Moreover, as can be seen from the spatial distribution of positive bias dI/dV maps of 7-aGNR on both surfaces [Figs. 2(c) and 2(f)], the maps of the pure armchair resonances ($R + n$) on Ag(111) can still be identified but they are modulated by other tunneling channel contributions that we attribute to the presence of interface resonances/states (IRs) between 7-aGNR and Ag(111) as discussed later in Sec. III D.

To understand the tunneling electronic excitations behavior in the 7-aGNRs on Ag(111) surface, we have systematically

recorded the dI/dV maps at different tunneling resonances for different 7-aGNR lengths. The corresponding spatially mapped tunneling excitations presented in Fig. 3 clearly allow the visualization of 7-aGNR length vs electronic stabilization on Ag(111) surface. The plot of the energy eigenvalues defining the quasiparticle gaps (V_{bias} of $R \pm 1$) against the 7-aGNR length on both Ag(111) and Au(111) surfaces clearly showcases the gap evolution that follows the $\sim 1/L^2$ dependence [except $R - 1$ on Ag(111)], where “ L ” is the length of the 7-aGNR [Figs. 4(a) and 4(b)] [31]. Notice that a single cyclodehydrogenated monomer was only observed on Au(111) surface but not on Ag(111). This leads to the observed deviation in the $R \pm 1$ resonances energies for a cyclodehydrogenated single DBBA monomer unit on Au(111) surface [Fig. 4(b)]. For 7-aGNRs longer than two monomer units, an intrinsic confinement effect gives rise to a decrease of the quasiparticle resonances with increasing length of 7-aGNR. With quasiparticle resonances varying as a function of $1/L^2$, it should be noted that these energetic positions of STS measured electronic resonances certainly includes the substrate induced electronic structure renormalization effects in addition to the GNR size-related confinement effects. One such substrate surface related phenomenon can be directly seen by plotting the stabilized 7-aGNR tunneling resonance energetic positions against the work function of Ag(111) and Au(111) surfaces [~ 5.3 eV for Au(111) and ~ 4.7 eV for Ag(111)] [32]. A clear relative positioning offset of ~ 0.9 eV in the HOMO and LUMO electronic resonances of a 7-aGNR with respect to the E_F of two different surfaces can be visualized in Fig. 4(c).

B. Edge states of 7-aGNRs on Ag(111) and Au(111) surfaces

Another impact of the substrate surface work function difference on the 7-aGNR is its ESs electronic configurations, which are localized at the zigzag structure termini [2,33,34]. On Ag(111), the low-bias ESs (RE1) are located at ~ -450 mV and remain unchanged as a function of 7-aGNR length beyond two-monomer units [Fig. 5(a); see Supplemental Material [25] Sec. 2 for more details]. This indicates negligible longitudinal electronic interactions between the two zigzag edges through the 7-aGNR chemical structure. On Au(111), these ESs are located at $\sim +20$ mV, in perfect agreement with the values reported in the literature [Fig. 5(b)] [2]. The detailed dI/dV spectra and maps presented in Figs. 5(a) and 5(b) compare with a good match the typical low-bias ES characteristics of a 7-aGNR on Ag(111) and Au(111) surfaces.

On Ag(111), the end position of a 7-aGNR also revealed an extra broad dI/dV resonance centered at $\sim +1.25$ V [Fig. 5(c)]. The corresponding dI/dV map exhibits a new ES character (RE2) located at both ends of the 7-aGNR [Fig. 5(c), lower panel]. Interestingly, its differential conductance maxima coincide with the central carbon (C) atom position at the zigzag termini, unlike the low bias ES (RE1), the maxima of which are located at the outermost C atoms. Moreover, this new high-bias ES map coincides with the regular $R + n$ eigenmode of the 7-aGNR on Ag(111). Similar high-bias dI/dV measurements carried out at both ends of the 7-aGNR on Au(111) also captured the onset of an additional and new

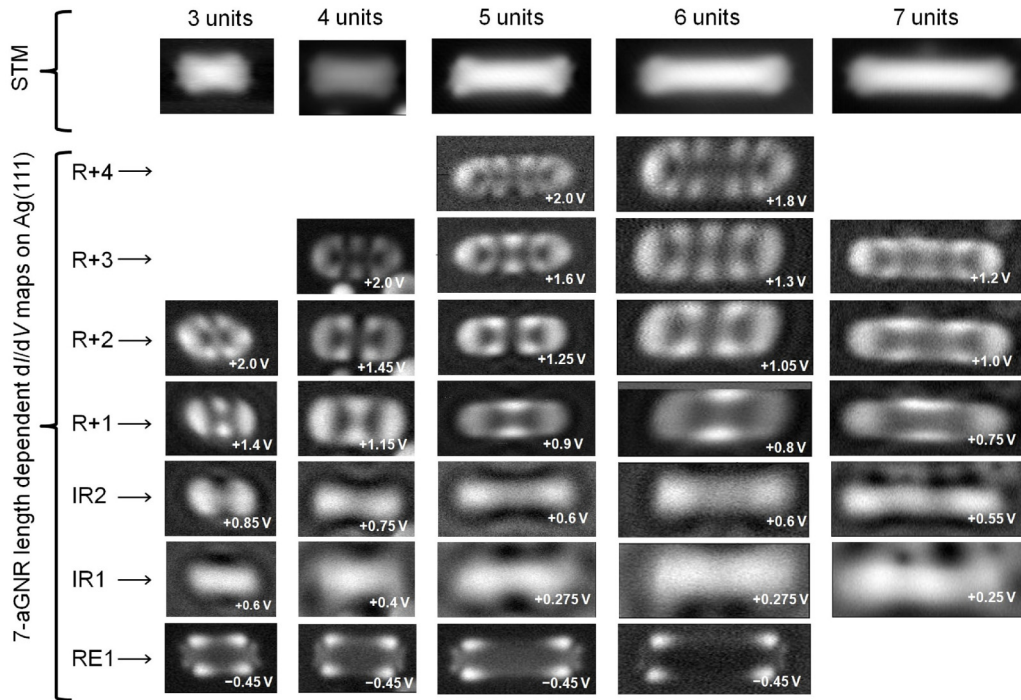


FIG. 3. Spatial dI/dV mapping of tunneling electronic excitations in 7-aGNRs on Ag(111). STM images (top row) and dI/dV maps (columns) recorded at different bias voltages for different lengths of 7-aGNR on Ag(111) surface. Corresponding 7-aGNR lengths are given in number of DBBA monomer units on top of STM images. Different electronic eigenmodes ($R + n$, IRn , and RE1) are indicated in the figure. Tunneling bias voltage for each dI/dV map is indicated in the inset of the corresponding map.

ES resonance at +2.3 V [Fig. 5(d)]. The corresponding dI/dV map consistently shows a large differential conductance coinciding with the central C position at the zigzag termini. Moreover, similar to the low-bias ESs, these new high-bias ESs are also found to be independent of the 7-aGNR length on both Ag(111) and Au(111) (see Supplemental Material [25] Sec. 2 for more details). They are the positive bias equivalent to the $R - 1$ topological length invariant mono-electronic contribution of the 7-aGNR STS resonance observed at -1.7 V on Ag(111). Surprisingly, in spite of numerous and extensive

studies of 7-aGNR on Au(111), no such high-bias ES characteristic was reported so far on Au(111).

The neutral electronic ground state of an unsupported 7-aGNR can be described in first approximation by a single Slater determinant like electronic configuration where half of its delocalized molecular orbitals are filled up, while each edge-localized SOMO is half full with an antiferromagnetic coupling between the unpaired electrons at both ends [11,28,33]. When adsorbed on a metallic surface, this neutral electronic ground state configuration of 7-aGNR (including

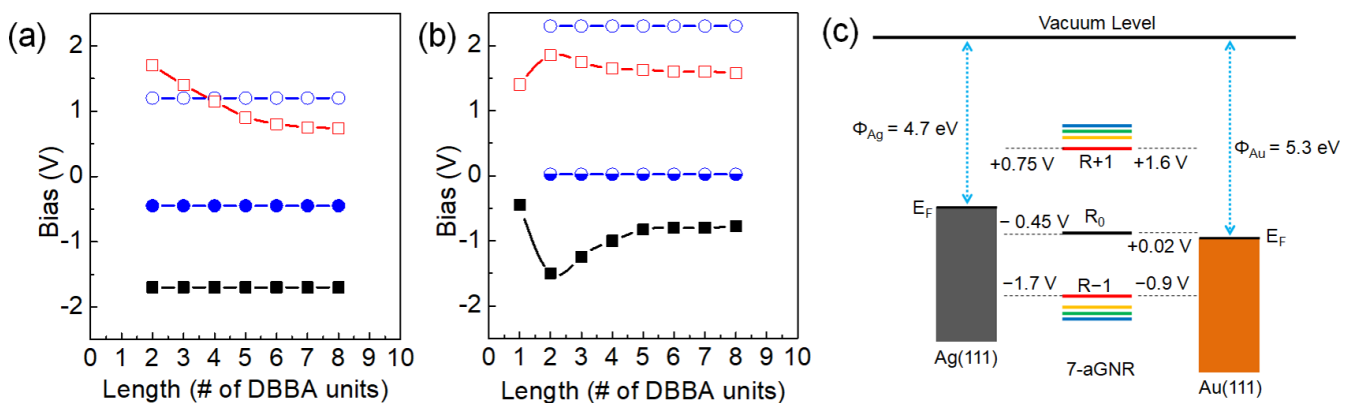


FIG. 4. Electronic energy level structure of a 7-aGNR on Ag(111) and Au(111) surfaces. Electronic stabilization behavior visualized for the quasiparticle resonances of $R + 1$ (open red squares) and $R - 1$ (filled black squares), which contribute the quasiparticle-electronic band gaps of a 7-aGNR (a) on Ag(111) and (b) on Au(111), respectively. ES resonance positions of 7-aGNR, RE1 [(half) filled blue circles], and RE2 (open blue circles), are also presented in the figures for reference. (c) Schematic illustration of the relative positioning of different tunneling electronic excitation energies extracted from the dI/dV spectra of a stabilized 7-aGNR visualized with respect to the Fermi levels of Ag(111) and Au(111) surfaces.

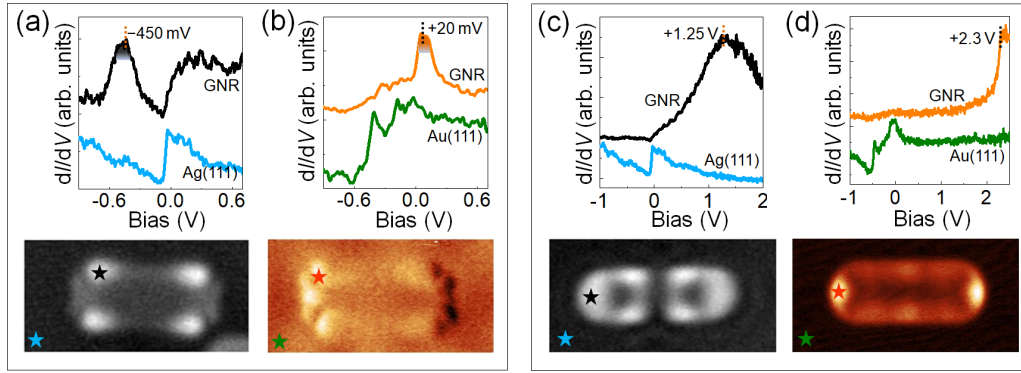


FIG. 5. Edge localized electronic characteristics of 7-aGNRs. (a) A typical dI/dV spectrum (upper panel, black curve) and corresponding dI/dV map (lower panel) showing the low-bias ES around -450 mV of a five-monomer-units-long 7-aGNR on Ag(111) surface. Similarly, the dI/dV spectrum and map presented in (b) illustrate the same low-bias 7-aGNR ES characteristic (orange curve) located at $+20$ mV on Au(111) surface. (c), (d) Wide range dI/dV characteristics revealing a new high-bias ES of 7-aGNR located at $\sim +1.25$ V on Ag(111) surface [(c), black curve] and at $+2.3$ V on Au(111) surface [(d), orange curve]. Corresponding dI/dV maps in the lower panels show the characteristic appearance of high-bias ESs of 7-aGNR on Ag(111) and Au(111) surfaces, respectively. Scan areas are $8 \text{ nm} \times 4 \text{ nm}$ (length \times height). Ag(111) and Au(111) reference dI/dV spectra are presented in blue and green curves, respectively.

the SOMOs) is realigned in energy with respect to E_F and undergoes an oxidation or reduction mechanism depending on the chemical potential of the metallic surface. As presented in Fig. 5(a), the SOMO-like resonances (RE1) of 7-aGNR on Ag(111) are located well below E_F (-450 mV). As a consequence, a 7-aGNR on Ag(111) is electronically fully reduced at both zigzag termini with its two SOMOs being completely filled up. Therefore, the ground state resonance of this charged 7-aGNR (RE1 at -0.45 V) on Ag(111) is the result of a single hole transfer process through each edge of 7-aGNR via the SOMO channels. On Au(111), the same 7-aGNR ESs were found at $+20$ mV above E_F [Fig. 5(b)]. In a first approximation, the modified 7-aGNR ground state on Au(111) corresponds to the electronic oxidation at both zigzag termini with its two SOMOs in an almost empty configuration. The RE1 resonance at $+20$ mV is therefore the result of a single electron transfer process through the 7-aGNR via the new empty configuration of the SOMO channels. Clearly, the observed RE1 of a 7-aGNR on Au(111) is no more the ground state resonance while it is now determined by the first resonance (R -1) captured at negative bias [at -0.90 V in Fig. 2(e)].

The work function difference [~ 5.3 eV for Au(111) and 4.7 eV for Ag(111)] [32] is decisive for stabilizing different 7-aGNR ground states [Fig. 4(c)]. But, the edge-localized SOMO resonances (RE1) are robust irrespective of the substrate materials, as seen in Figs. 5(a) and 5(b). The RE1 dI/dV maps on both surfaces are nevertheless quantitatively different because the energetic position ($+20$ mV) on Au(111) is too close to the E_F for the SOMO to be totally quantum empty. On Ag(111), the SOMO at -450 mV is certainly filled up completely and thus leading to a better dI/dV contrast at both 7-aGNR edges as compared to Au(111).

C. Conformation of 7-aGNR on Ag(111) and Au(111)

As discussed above, the lower work function of Ag(111) brings the RE1 resonance well below E_F . As a consequence, the 7-aGNR on Ag(111) is electronically reduced by a filling

up of its two SOMO (at both zigzag termini) responsible for the RE1 resonance measured at -0.45 V. The stabilization of this resonance occurs for 7-aGNR length above two-monomer units. To simulate this SOMO electronic effect by semiempirical calculations including the molecular mechanics for the curvature, the minimum energy conformation of a five-monomer-units-long 7-aGNR was calculated on Ag(111) and Au(111) by removing or adding one central hydrogen (H) atom at each zigzag terminus of the 7-aGNR. The surface conformation of 7-aGNR was optimized in ASEd+ [35] by taking into account the underlying bulk metallic surface. For reference, the conformation of an intact 7-aGNR was first optimized on both the Ag(111) and Au(111) surfaces. These reference calculations result in a perfectly planar conformation of 7-aGNR on both surfaces [Fig. 6(a)] [35].

By removing one H atom at each zigzag terminus, the ASEd+ optimization leads to a curved conformation of 7-aGNR on Ag(111) [Fig. 6(b)]. To simulate the opposite case, i.e., a 7-aGNR oxidation on Au(111), one H atom was added at each edge that creates an sp^3 configuration at the central C position of the zigzag termini. This sp^3 end configuration is equivalent to the removal of one electron per SOMO. In this second case, the optimized five-monomer-unit-long 7-aGNR on Au(111) was found to be strictly flat, according to ASEd+ [Fig. 6(c)].

Experimental lateral STM molecular manipulations of 7-aGNR were also attempted to verify the possibility of a native chemical bond formation between the end positions of the 7-aGNR and the metallic surface or, alternatively, the bonding of a metal adatom during the on-surface synthesis process, for example at the site of a missing H atom at one edge [36,37], which could possibly stabilize the curved conformation on Ag(111). Our on-surface synthesized 7-aGNRs are easily manipulated from one stable position to the next one on both surfaces with standard STM manipulation conditions (junction resistance: $400 \text{ k}\Omega$), therefore confirming the absence of any chemical bond formation.

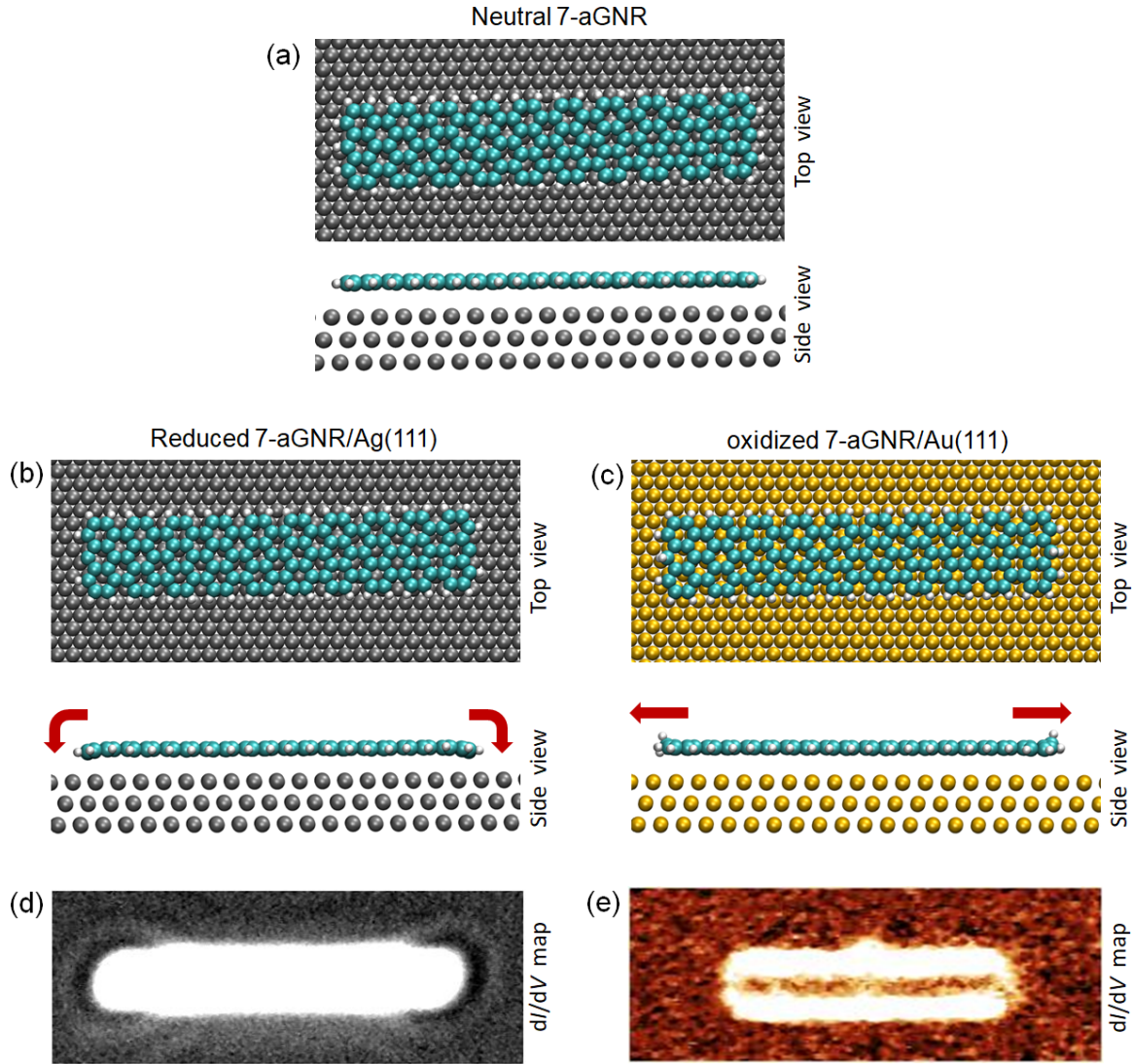


FIG. 6. 7-aGNR conformations on Ag(111) and Au(111). (a) Minimum energy configuration of a neutral five-monomer-units-long 7-aGNR revealing a flat conformation after relaxing its structure on the Ag(111) surface calculated by ASED+. The flat conformation shown in top (top panel) and side (bottom panel) views is used here as a reference. (b) Calculated minimum energy conformation of a reduced 7-aGNR on Ag(111) surface after removing one H atom at each zigzag terminus. It shows a marked downward curvature at both termini. (c) Calculated minimum energy conformation of an oxidized 7-aGNR on Au(111) after adding one H atom at each zigzag terminus. After a complete geometry optimization, the curvature of 7-aGNR, $\Delta z = \langle z_c \rangle - \langle z_{\text{edge}} \rangle$, on Ag(111) is $\sim 0.455 \text{ \AA}$ and on Au(111) surface is $\sim 0.00 \text{ \AA}$. Here, $\langle z_c \rangle$ and $\langle z_{\text{edge}} \rangle$ stand for height (z) of the 7-aGNR center and edge carbon atom heights, respectively, relative to the surface metal atoms. (d), (e) Experimental dI/dV maps corresponding to the (b) and (c) configurations that reveal the presence, in (d), and absence, in (e) of circular patterns at the 7-aGNR edge positions on Ag(111) and Au(111), respectively. Scan parameters are $\sim +600 \text{ mV}/100 \text{ pA}$. Scan sizes are $15 \text{ nm} \times 5.5 \text{ nm}$ (length \times height).

D. Lateral quantization of the Ag(111) Shockley surface states at the 7-aGNR/Ag(111) interface

One consequence of the curved 7-aGNR conformation on Ag(111) is that both ends behave as scattering centers [10] for the two-dimensional (2D) surface electron gas of Ag(111). Indeed, on Ag(111), circular standing waves can be clearly observed, for example at $+600 \text{ mV}$ around the two 7-aGNR ends, with a maximum scattering strength concentrated at the end positions as presented in Fig. 6(d) (see Supplemental Material [25] Sec. 3 for more details). In contrast, such scattering effects were not observed on the Au(111) surface [Fig. 6(e)].

Another consequence of the 7-aGNR curvature is the formation of a 2D rectangular quantum box at the interface between the 7-aGNR and the Ag(111) surface, in between the two 7-aGNR ends. In contrast to the Au(111) case, the two supplementary interface resonances (IR1 and IR2) captured at $+0.275$ and $+0.6 \text{ V}$ on Ag(111) [in Fig. 2(b)] and their corresponding dI/dV maps [IR1 and IR2 in Fig. 2(c)] are coming from the eigenmodes of this interfacial quantum box.

To confirm this interpretation, dI/dV spectra were recorded exactly at the central location of the 7-aGNR box, and also for different lengths to change the effective size of

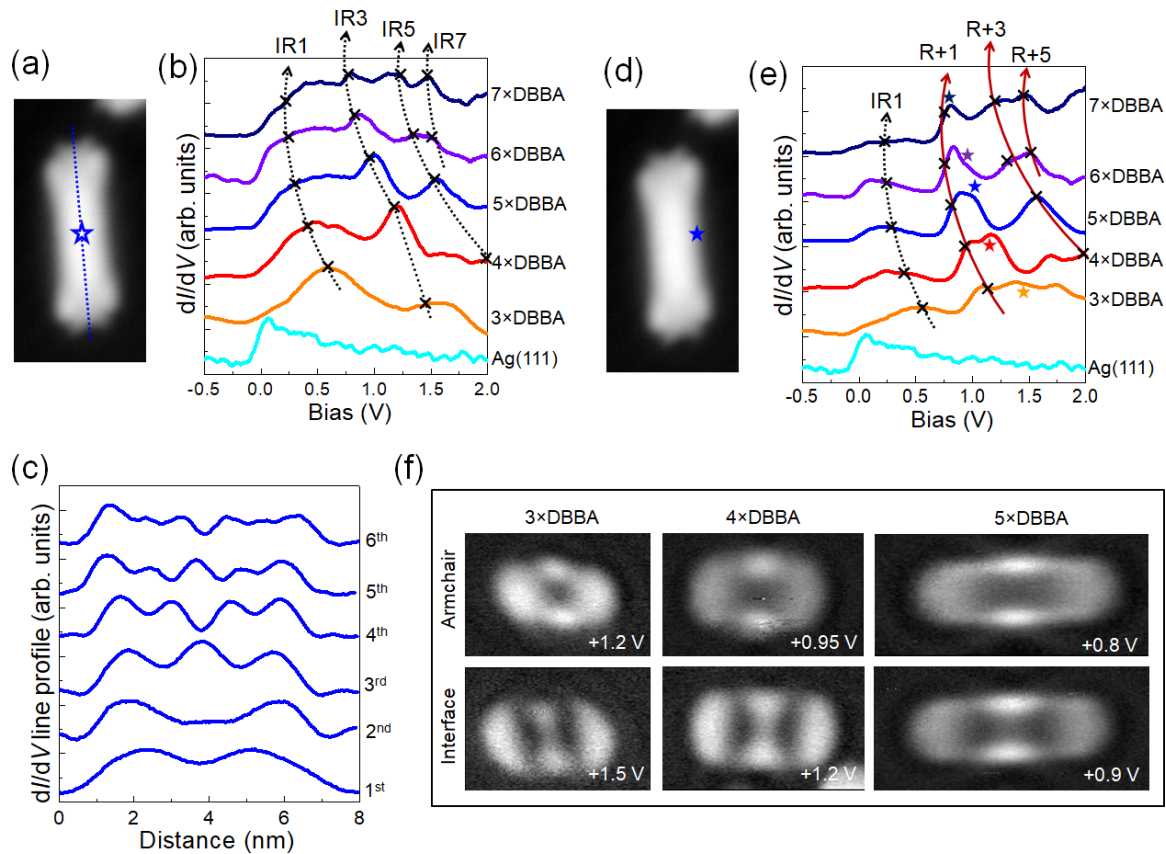


FIG. 7. Shockley surface state lateral quantization at the interface of 7-aGNR and Ag(111) surface. (a) STM image showing the spectroscopic position (open blue star symbol) and (b) corresponding dI/dV spectra reveal the length dependency of several electronic interfacial resonances (IRs). In (b) each electronic resonance can be followed as a function of the 7-aGNR length as indicated by the dotted arrows. (c) Line profiles extracted from the dI/dV maps of five-monomer-units-long 7-aGNR [from Fig. 1(c)] along the central axis as indicated by dotted line in (a). These profiles reveal the laterally quantized standing-wave-like behavior of IRs. (d) STM image showing the spectroscopic position at the armchair side center (closed blue star symbol) and (e) Corresponding dI/dV spectra of 7-aGNR revealing the intrinsic armchair side electronic eigenmode resonances ($R1$, $R + 3$, etc.) and their GNR length dependency. In (e) the shift of each armchair mode electronic resonance is indicated by the solid arrows. The shoulder peak (indicated with filled colored stars) represents the third quantized IR. An energetically isolated interface mode (IR1) was indicated with dotted arrow. (f) dI/dV maps recorded at different voltages comparing the first armchair resonance (top panels) and third quantized IR (bottom panels) for different 7-aGNR lengths revealing the well isolated and nonhybridized armchair and IR modes.

this quantum cavity [Figs. 7(a) and 7(b)]. As the length of the 7-aGNR increases, all the dI/dV resonances recorded at the central position of 7-aGNR are downshifted in voltage [as indicated by dotted arrows in Fig. 7(b)]. On the other hand, the line profiles extracted from positive bias dI/dV maps of the five-monomer-units-long 7-aGNR [Fig. 2(c)] and plotted in Fig. 7(c) clearly depict the standing wave pattern with its increasing number of nodes as a function of the bias voltage. These characteristic features can be attributed to the lateral quantization of Ag(111) surface electrons at the 2D interface quantum box. By construction, we monitor here the odd eigenmode series (first, third, fifth, etc.) of the quantized IRs since the dI/dV spectra presented in Fig. 7(b) are recorded at the central position on the 7-aGNR.

To elucidate the mixing between the quantized IRs and the intrinsic 7-aGNR resonances ($R + n$) on Ag(111), the dI/dV spectra recorded at the armchair side (center location) can be compared for different 7-aGNR lengths [Figs. 7(d) and 7(e)]. A close inspection of the dI/dV spectra reveals an extra shoulder resonance at +1.5 V for three-monomer-units-long

7-aGNR [indicated with star symbols in Fig. 7(e)] in addition to the intrinsic resonances (indicated with solid arrows). As the length increases, this particular shoulder resonance clearly exhibits a more modest shift toward lower bias voltage than the intrinsic resonances before eventually coinciding with the first intrinsic tunneling excitation resonance ($R + 1$ at +0.75 V) at the seven-monomer-units-long 7-aGNR. In Fig. 7(f), the dI/dV maps are recorded at the additional shoulder resonance and at the first intrinsic resonance ($R + 1$) for three-, four-, and five-monomer-long 7-aGNRs. These maps clearly show the absence of any hybridization between the armchair and quantized IR resonances, as can be seen from energetically deconvoluted armchair $R + 1$ eigenmode from the interface IR3 eigenmode. The isolated nature of armchair and quantized IR modes with the absence of central IR fringes in the former compared to the latter can be clearly seen for shorter GNR lengths due to their different energetic positions [Fig. 7(f)]. As the length of a GNR increases, the mixing of both eigenmodes at similar bias voltages lead to the complexity in resolving them in STS mappings. Moreover, these two

distinct eigenmodes are spatially separated as well since the origin of armchair modes are intrinsic to a 7-aGNR chemical structure backbone while the interface modes are exclusive to the vacuum cavity formed between the Ag(111) and curved 7-aGNR molecule. Note that similar measurements carried out on Au(111) do not exhibit any interface patterns as can be seen from the dI/dV maps presented in Fig. 2(f), where the central part of $R + n$ eigenmodes along the 7-aGNR length remains featureless.

IV. CONCLUSIONS

In conclusion, the tunneling electronic excitation spectra for a 7-aGNR on Ag(111) surface are complex, yet we have successfully deconvoluted the different contributions by systematically correlating, for a 7-aGNR of identical length, the modal landscape on Ag(111) with its equivalent on Au(111) used as a reference surface. In particular, this comparison provides substantial evidence, which is further supported by the theoretical calculations, that the charge transfer between ESs and metallic support surface results in a curved 7-aGNR conformation on the Ag(111) surface but not on the Au(111) surface. The curved conformation creates a 2D quantum-box-like cavity that exhibits laterally quantized Shockley surface states at the interface between the 7-aGNR and the metallic

surface. The lower work function of Ag(111) pushes the 7-aGNR ESs below the Fermi level where the intrinsic tunneling electronic excitations significantly entangle with the interfacial Shockley states. As a result, we show that the spatially mapped 7-aGNR tunneling excitations cannot be interpreted solely as its intrinsic electronic character but rather as the complex mixing of intrinsic molecular electronic features with support surface related phenomena. Our work on the 7-aGNR provides a generic methodological approach to disentangle both aspects and finally reach out for the intrinsic molecular electronic resonances.

ACKNOWLEDGMENTS

U.T. acknowledges the H2020 Marie Skłodowska-Curie Actions for a Marie Curie Individual Fellowship (Grant No. 895239, GNR CONDUCTANCE). This work was also supported by the European Union Horizon 2020 FET open project “Mechanics with Molecules” (MEMO, Grant No. 766864), the University Paul Sabatier (Toulouse, France) and CNRS (France). Calculations were supported by a granted access to the HPC resources of CALMIP supercomputing center under the allocation 2022-P083. C.J. also acknowledges the support of the International Center of Materials Nanoarchitectonics (WPI-MANA), MEXT, Japan.

-
- [1] P. Ruffieux, J. Cai, N. C. Plumb, L. Patthey, D. Prezzi, A. Ferretti, E. Molinari, X. Feng, K. Müllen, C. A. Pignedoli, and R. Fasel, Electronic structure of atomically precise graphene nanoribbons, *ACS Nano* **6**, 6930 (2012).
 - [2] M. Koch, F. Ample, C. Joachim, and L. Grill, Voltage-dependent conductance of a single graphene nanoribbon, *Nat. Nanotechnol.* **7**, 713 (2012).
 - [3] S. Linden, D. Zhong, A. Timmer, N. Aghdassi, J. H. Franke, H. Zhang, X. Feng, K. Müllen, H. Fuchs, L. Chi, and H. Zacharias, Electronic Structure of Spatially Aligned Graphene Nanoribbons on Au(788), *Phys. Rev. Lett.* **108**, 216801 (2012).
 - [4] N. Kharche and V. Meunier, Width and crystal orientation dependent band gap renormalization in substrate-supported graphene nanoribbons, *J. Phys. Chem. Lett.* **7**, 1526 (2016).
 - [5] T. Wang, A. B. Layunta, N. Friedrich, M. V. Varela, J. P. Calupitan, J. I. Pascual, D. Peña, D. Casanova, M. Corso, and D. G. de Oteyza, Aza-triangulene: On-surface synthesis and electronic and magnetic properties, *J. Am. Chem. Soc.* **144**, 4522 (2022).
 - [6] U. Thupakula, X. Bouju, J. Castro-Esteban, E. Dujardin, D. Peña, and C. Joachim, Planar bridging an atomically precise surface trench with a single molecular wire on an Au(111) surface, *Chem. Phys. Lett.* **806**, 140029 (2022).
 - [7] L. Talirz, P. Ruffieux, and R. Fasel, On-surface synthesis of atomically precise graphene nanoribbons, *Adv. Mater.* **28**, 6222 (2016).
 - [8] Z. Xiao, C. Ma, W. Lu, J. Huang, L. Liang, K. Hong, A. P. Li, B. G. Sumpter, and J. Bernholc, Ab initio investigation of the cyclodehydrogenation process for polyanthrylene transformation to graphene nanoribbons, *npj Comput. Mater.* **5**, 91 (2019).
 - [9] J. B. Neaton, M. S. Hybertsen, and S. G. Louie, Renormalization of Molecular Electronic Levels at Metal-Molecule Interfaces, *Phys. Rev. Lett.* **97**, 216405 (2006).
 - [10] L. Gross, F. Moresco, L. Savio, A. Gourdon, C. Joachim, and K. H. Rieder, Scattering of Surface States Electrons by Large Organics Molecules, *Phys. Rev. Lett.* **93**, 056103 (2004).
 - [11] S. Wang, L. Talirz, C. A. Pignedoli, X. Feng, K. Müllen, R. Fasel, and P. Ruffieux, Giant edge state splitting at atomically precise graphene zigzag edges, *Nat. Commun.* **7**, 11507 (2016).
 - [12] Y. Que, B. Liu, Y. Zhuang, C. Xu, K. Wang, and X. Xiao, On-surface synthesis of graphene nanoribbons on two-dimensional rare earth–gold intermetallic compounds, *J. Phys. Chem. Lett.* **11**, 5044 (2020).
 - [13] M. Kolmer, A. K. Steiner, I. Izydorczyk, W. Ko, M. Engelund, M. Szymanski, A. P. Li, and K. Amsharov, Rational synthesis of atomically precise graphene nanoribbons directly on metal oxide surfaces, *Science* **369**, 571 (2020).
 - [14] R. Zuzak, J. C. Esteban, M. Engelund, D. Pérez, D. Peña, and S. Godlewski, On-surface synthesis of nanographenes and graphene nanoribbons on titanium dioxide, *ACS Nano* **17**, 2580 (2023).
 - [15] I. Swart, P. Liljeroth, and D. Vanmaekelbergh, Scanning probe microscopy and spectroscopy of colloidal semiconductor nanocrystals and assembled structures, *Chem. Rev.* **116**, 11181 (2016).
 - [16] J. Yang, D. Sordes, M. Kolmer, D. Martrou, and C. Joachim, Imaging, Single atom contact and single atom manipulations at low temperature using the new scienta omicron LT-UHV-4 STM, *Eur. Phys. J. Appl. Phys.* **73**, 10702 (2016).
 - [17] J. Cai, P. Ruffieux, R. Jaafar, M. Bieri, T. Braun, S. Blankenburg, M. Muoth, A. P. Seitsonen, M. Saleh, X. Feng, K.

- Müllen, and R. Fasel, Atomically precise bottom-up fabrication of graphene nanoribbons, *Nature (London)* **466**, 470 (2010).
- [18] A. B. Anderson, Electron density distribution functions and the ASED–MO theory, *Int. J. Quantum Chem.* **49**, 581 (1994).
- [19] M. Bosson, C. Richard, A. Plet, S. Grudinin, and S. Redon, Interactive quantum chemistry: A divide-and-conquer ASED–MO method, *J. Comput. Chem.* **33**, 779 (2012).
- [20] F. Ample and C. Joachim, A semi-empirical study of polyacene molecules adsorbed on a Cu(110) surface, *Surf. Sci.* **600**, 3243 (2006).
- [21] C. J. Villagómez, F. Castanié, C. Momblona, S. Gauthier, T. Zambelli, and X. Bouju, Adsorption of single 1,8-octanedithiol molecules on Cu(100), *Phys. Chem. Chem. Phys.* **18**, 27521 (2016).
- [22] U. G. E. Perera, F. Ample, H. Kersell, Y. Zhang, G. Vives, J. Echeverria, M. Grisolia, G. Rapenne, C. Joachim, and S.-W. Hla, Controlled clockwise and anticlockwise rotational switching of a molecular motor, *Nat. Nanotechnol.* **8**, 46 (2013).
- [23] Y. Makoudi, E. Duverger, M. Arab, F. Chérioux, F. Ample, G. Rapenne, X. Bouju, and F. Palmino, Room-temperature electronic template effect of the SmSi(111) – 8×2 interface for self-alignment of organic molecules, *Chem. Phys. Chem.* **9**, 1437 (2008).
- [24] C. J. Villagómez, F. Buendía, L. O. Paz-Borbón, B. Fuentes, T. Zambelli, and X. Bouju, Surface vacancy generation by STM tunneling electrons in the presence of indigo molecules on Cu(111), *J. Phys. Chem. C* **126**, 14103 (2022).
- [25] See Supplemental Material at <http://link.aps.org/supplemental/10.1103/PhysRevMaterials.7.085005> for more details on the 7-aGNR length independent negative bias STS resonance behavior on Ag(111), edge state dI/dV characteristics of 7-aGNR on Ag(111) and Au(111), and 7-aGNR edge states interaction behavior with metallic surfaces.
- [26] M. Portais and C. Joachim, Hole-electron quantum tunnelling interferences through a molecular junction, *Chem. Phys. Lett.* **592**, 272 (2014).
- [27] F. Eisenhut, T. Kühne, F. García, J. M. Alonso, E. Guitián, G. Trinquier D.Pérez, G. Cuniberti, C. Joachim, D. Peña, and F. Moresco, Dodecacene generated on surface: A re-opening of the energy gap, *ACS Nano* **14**, 1011 (2020).
- [28] R. S. K. Houtsma, J. Rie, and M. Stöhr, Atomically precise graphene nanoribbons: Interplay of structural and electronic properties, *Chem. Soc. Rev.* **50**, 6541 (2021).
- [29] H. Söde, L. Talirz, O. Göning, C. A. Pignedoli, R. Berger, X. Feng, K. Müllen, R. Fasel, and P. Ruffieux, Electronic band dispersion of graphene nanoribbons via Fourier-transformed scanning tunneling spectroscopy, *Phys. Rev. B* **91**, 045429 (2015).
- [30] Our STS investigation reveals that the -1.7 V resonance is GNR length independent. A detailed calculation revealed that it is due to an intrinsic topological length invariant holelike mono-electronic state contribution creating this STS resonance captured at ~ -1.7 V. A detailed manuscript based on these calculations is currently under preparation.
- [31] L. Talirz, H. Söde, S. Kawai, P. Ruffieux, E. Meyer, X. Feng, K. Müllen, R. Fasel, C. A. Pignedoli, and D. Passerone, Band gap of atomically precise graphene nanoribbons as a function of ribbon length and termination, *Chem. Phys. Chem.* **20**, 2348 (2019).
- [32] H. B. Michaelson, The work function of the elements and its periodicity, *J. Appl. Phys.* **48**, 4729 (1977).
- [33] K. Nakada, M. Fujita, G. Dresselhaus, and M. S. Dresselhaus, Edge state in graphene ribbons: Nanometer size effect and edge shape dependence, *Phys. Rev. B* **54**, 17954 (1996).
- [34] C. Bronner, F. Leyssner, S. Stremlau, M. Utecht, P. Saalfrank, T. Klamroth, and P. Tegeer, Electronic structure of a subnanometer wide bottom-up fabricated graphene nanoribbon: End states, band gap, and dispersion, *Phys. Rev. B* **86**, 085444 (2012).
- [35] F. Eisenhut, T. Kühne, J. Monsalve, S. Srivastava, D. A. Ryndyk, G. Cuniberti, O. Aiboudi, F. Lissel, V. Zobač, R. Robles, N. Lorente, C. Joachim, and F. Moresco, One-way rotation of a chemically anchored single molecule-rotor, *Nanoscale* **13**, 16077 (2021).
- [36] J. van der Lit, M. P. Boneschanscher, D. Vanmaekelbergh, M. Ijäs, A. Uppstu, M. Ervasti, A. Harju, P. Liljeroth, and I. Swart, Suppression of electron–vibron coupling in graphene nanoribbons contacted via a single atom, *Nat. Commun.* **4**, 2023 (2013).
- [37] L. Talirz, H. Söde, J. Cai, P. Ruffieux, S. Blankenburg, R. Jafaar, R. Berger, X. Feng, K. Müllen, D. Passerone, R. Fasel, and C. A. Pignedoli, Termini of bottom-up fabricated graphene nanoribbons, *J. Am. Chem. Soc.* **135**, 2060 (2013).